Multi-scale lumped modeling of micro-channels cooling structure for W7-X divertor unit target module

Fusion Engineering and Design 204 (2024) 114481

Contents lists available at ScienceDirect

Fusion Engineering and Design

journal homepage: www.elsevier.com/locate/fusengdes

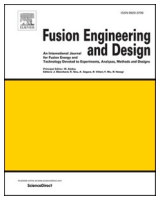

# Multi-scale lumped modeling of micro-channels cooling structure for W7-X divertor unit target module

Francesco Carrone [a], Rosa Difonzo [a], Joris Fellinger [b], Laura Savoldi [a,*]

[a] Dipartimento Energia «Galileo Ferraris», Politecnico di Torino, Turin, Italy
[b] Max-Planck-Institute for Plasma Physics, Greifswald, Germany

ARTICLE INFO

*Keywords:*
Divertor
Micro-channels
Numerical modeling
Thermo-mechanics
Thermo-hydraulics
Lumped modeling

ABSTRACT

A novel concept for the cooling system of the W7-X divertor unit target module has been proposed, which involves tiles equipped with parallel arrays connected by hundreds of sub-millimeter rectangular micro-channels (MCs), obtained using Additive Manufacturing techniques. The structural material proposed for the heat sink substrate is galvanized copper, while the plasma facing material is tungsten. To reduce the high computational cost of thermal-hydraulic simulations of the tiles, a multi-scale lumped modeling approach has been built in previous studies. This involves replacing a group of hydraulic parallel MCs with a porous strip (PS), suitably calibrated to reproduce similar thermal-hydraulic behavior of the MCs. The aim of the current work is to verify that the PS-model is also suitable for the thermo-mechanical stress evaluation, comparing the results from arrays with MCs and PS. Since the heat sink and plasma-facing tiles are bonded, the interfacial delamination and shear stresses are analyzed, being crucial for structural integrity. The analyses, carried out in the elastic regime, show that the PS model returns conservative results when compared to the MCs model, with an overestimation of the delamination and shear stresses at the free edge. Results from both models reveal nearly identical interfacial stress predictions at the free surface edge. Moreover, it is found that both MCs and PS blocks, located near the bond interface, contribute to high-stress fluctuations that could lead to the delamination of the bond interface, suggesting that the distance of the microchannel from the interface should be increased. The PS model can reliably be used to design and verify the most convenient series/parallel connection of the tiles in the divertor unit target module, taking operational constraints into consideration.

## 1. Introduction

Fusion energy could in principle play a role in decarbonizing our economies, as it can potentially provide a nearly limitless source of clean and sustainable energy [1], although in the long run [2]. Considering the magnetic confinement, stellarators are taken into consideration because of the benefit of avoiding the disadvantages of pulsed operation intrinsic in the tokamak configuration [3]. This study notably focuses on the Wendelstein 7-X (W7-X), an achievement of the Max-Planck-Institute for Plasma Physics (IPP) in Greifswald. The highest interest is in the novel water-cooled divertor development [4], which consists of 10 similar discrete divertor units and is composed of target modules [5]. The target modules (TMs) are positioned in vertical and horizontal areas, defining the pumping gap, and covering a total area of 25.6 $m^2$ [6]; each TM is composed of target elements (TEs), made of flat tiles of the same length, placed onto a support frame and fed with water from manifolds [7]. The target heat flux to be removed is 10 $MW/m^2$ in nominal operating conditions.

Different solutions of the TEs cooling structure are explored; this work refers to the novel proposal of a network of parallel arrays of submillimeter rectangular channels, micro-channels (MCs), connected by Z-manifolds. The flat tile design (10 × 10 cm) consists of a galvanized copper heat sink (HS) and a 2 mm tungsten layer that is designed to withstand the uniformly distributed heat load of 10 $MW/m^2$. A schematic view is reported in Fig. 1. This complex geometry can be obtained thanks to the realization of plastic cooling channels by Additive Manufacturing (AM), and the plastic removal by acid or burning. The novel mockup has been investigated in [8], where a lumped modeling approach has been developed substituting the micro-channels with an equivalent porous medium, and used to carry out hydraulic and thermal analyses, to mitigate the high computational cost rising from the micro-channel structure. The approach in [8] prescribes the substitution

* Corresponding author.
*E-mail address:* laura.savoldi@polito.it (L. Savoldi).

https://doi.org/10.1016/j.fusengdes.2024.114481
Received 13 October 2023; Received in revised form 16 April 2024; Accepted 27 April 2024
Available online 11 May 2024

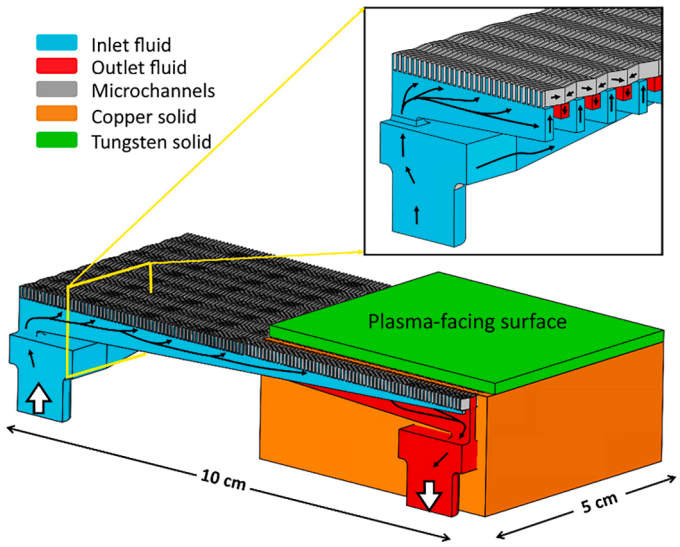


**Fig. 1.** Schematic view of the water-cooled divertor tile with the fluid path highlighted in the inset.

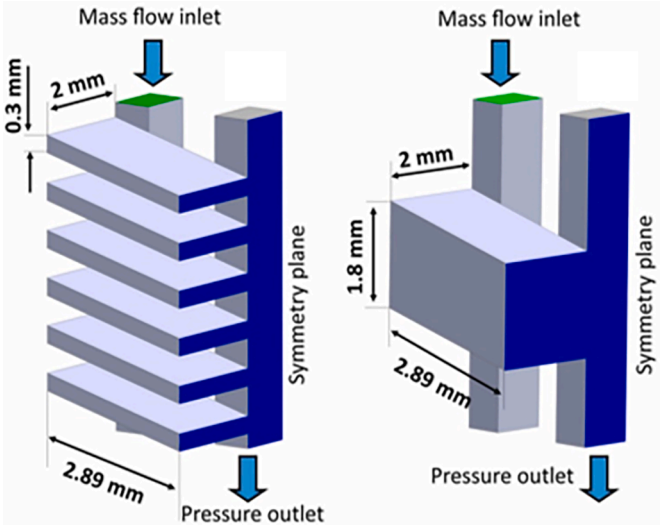


**Fig. 2.** Fluid subdomain of 6 parallel MCs (left figure) and the equivalent PS block (right figure).

of the detailed model with a Surrogate Model (SM), after a thermo-hydraulic calibration, and has been proven to be successful. The SM model adopts the principle of multi-scale modeling, replacing the detailed geometry of CFD with a coarser, appropriately calibrated scale to capture the key phenomena that describe the dominant behavior of the entire system in its entirety, as highlighted in [9].

This work aims to enhance the modeling strategy developed in [8] by assessing the thermo-mechanical behavior of the SM within the elastic regime, compared to the detailed model behavior once the calibration and validation of the SM is extended to heat fluxes up to 15 MW/m$^2$. Since the SM is demonstrated to well capture the thermal-hydraulic and thermal-mechanic behavior of the tile, ultimately it is used to assess different tile connections in a target module while keeping operational restrictions respected.

## 2. Methodology

Components such as the mockup considered in the current work require a huge effort in performing computational fluid dynamics (CFD)

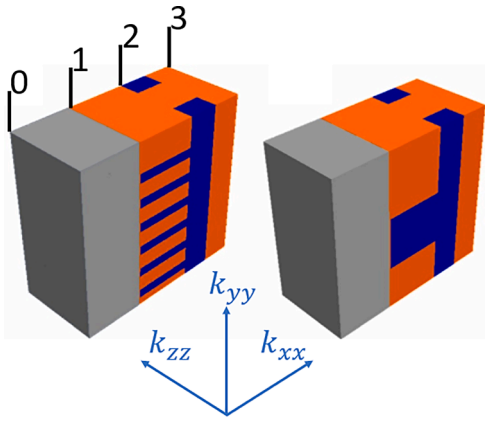


**Fig. 3.** MCs and PS-model with the number position of the surfaces where the KPIs are computed; also, the coordinate system of the anisotropic conductivity is reported.

analyses; in particular, solving the conjugate heat transfer problem is very computationally expensive because of the very fine computational grid implemented on the high number of MCs. To make the analyses affordable, a multi-scale lumped modeling approach using a SM is very helpful. In this case, a subdomain of 6 microchannels connected in parallel, the original component, is replaced by an equivalent Porous Strip (PS), the SM, as shown in Fig. 2. A proper calibration of the SM ensures that it reproduces the thermo-hydraulic behavior of the original model, as it can be checked by an appropriate validation exercise. The strategy for the development of the SM has been already highlighted in [8] and involves the analysis at different spatial scales. The first step considers a subdomain of the tile equipped with a few MCs. The hydraulic and thermal characterization of such subdomain is performed, covering a broad spectrum of mass flow rates, ranging from laminar to turbulent flow regimes. From them, the thermal-hydraulic characterization of the same subdomain equipped with the PS is performed. The porous medium viscous and inertia coefficients in the Darcy-Forchheimer formulation are found for the hydraulic behavior, and the thermal conductivity of the porous medium is computed to characterize the thermal behavior. The second step consists of the validation of the model developed at the micro-scale and considers this time an entire manifold of the tile, made by an array of 120 MCs (original component) and 20 PS blocks (SM). Thermal-hydraulic simulations are performed on the original and surrogate models, and the results are compared to assess the robustness of the SM. In Ref. [8], the different steps have been executed imposing a mass flow rate (for the entire tile) of 50 l/min, and a uniform heat flux of 5 MW/m$^2$ the tile aims to be tested in the GLADIS facility [10]. In the following sections, the thermal calibration (subdomain scale) and validation (array scale) are extended to cover a uniform heat flux up to 15 MW/m$^2$, while the hydraulic characterization, calibration and validation are unchanged with respect to what already shown in [8]. All the details on the hydraulic computational modelling are already given in [8].

A thermo-mechanical study is then introduced to verify whether the PS-model is suitable for the stress evaluation in comparison to the MCs-array. Therefore, finite element (FE) thermo-mechanical analyses are carried out, first on a relevant case study with a similar geometry of the MCs and PS array, and later on the considered arrays. In both cases the temperature maps are extracted from the thermal-hydraulic analyses and imposed as boundary condition in the thermo-mechanical simulation. All the simulations are performed using the commercial software STAR-CCM+ [11].

### 2.1. Thermal calibration

To perform the thermal calibration of the PS model, CFD simulations

**Table 1**
KPIs, outputs of the thermal-hydraulic simulation ($\dot{m} = 5.0$ **g/s**, $\dot{Q} = 15$ **MW/m²**) on the MCs subdomain used to calibrate the PS thermal conductivity.

| KPIs | value |
|---|---|
| $Q_H$ (W) | 24.5 |
| $Q_V$ (W) | 169 |
| $\Delta T_{ave,0}$ (K) | 578 |
| $\Delta T_{max,0}$ (K) | 585 |
| $\Delta T_{min,0}$ (K) | 575 |
| $\Delta T_{ave,1}$ (K) | 395 |
| $\Delta T_{ave,2}$ (K) | 341 |
| $\Delta T_{ave,3}$ (K) | 334 |

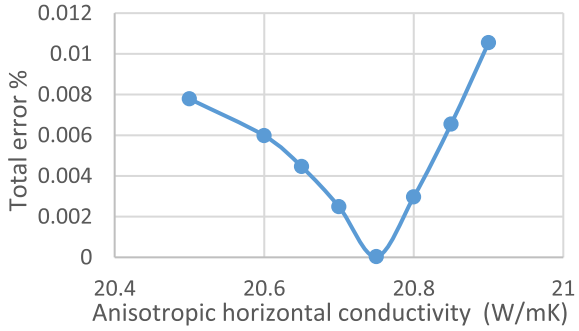


**Fig. 4.** Minimization of the total error computed on the heated surface to find the best fit anisotropic conductivity coefficient.

have been performed on the subdomain in Fig. 2 as detailed in [8], imposing a uniform heat flux of 15 MW/m² on the tungsten heated surface with a mass flow rate of 5.0 g/s. The absence of any local boiling in those conditions has been verified. The object of thermal calibration is to assess the equivalent thermal conductivity $k$ of the porous medium. It has been already observed in [8] that the best results are obtained considering $k$ anisotropic in view of the one-side heating configuration of the device.

As conjugate heat transfer analyses output, the horizontal (H) and vertical (V) thermal powers, $Q_H$ and $Q_V$, the first one entering the fluid from the tungsten layer and the second one entering the fluid from the copper layers within the MCs, are computed (see the computational domain in Fig. 3). The average, maximum, and minimum temperature on the heated surface ($\Delta T_{ave,0}$, $\Delta T_{max,0}$, $\Delta T_{min,0}$), the average temperature increase of the interface tungsten/copper ($\Delta T_{ave,1}$), of the interface copper/ manifold ($\Delta T_{ave,2}$) and of the back copper surface ($\Delta T_{ave,3}$) are computed as key performance indicators (KPIs). The results are reported in Table 1. The values of the anisotropic effective conductivity $k_{eff}^{aniso}$ are obtained as in Eq. (1),

$$\begin{cases} Q_H = k_{eff,H}^{aniso}\, x\, A_V\, x\, \dfrac{\partial T}{\partial h} \\ Q_V = k_{eff,V}^{aniso}\, x\, A_H\, x\, \dfrac{\partial T}{\partial v} \end{cases} \quad (1)$$

where $A_V$ and $A_H$ are the heat transfer surfaces for the H and the V heat flux, respectively and $\frac{\partial T}{\partial h}$ and $\frac{\partial T}{\partial v}$ are the H and V temperature gradients, respectively. According to the sketch in Fig. 3, $k_{eff,H}^{aniso}$ coincides with $k_{xx} = k_{zz}$, while $k_{eff,V}^{aniso}$with $k_{yy}$. Assuming the temperature gradients have almost the same value, the relation between the two thermal conductivity coefficients can be derived from Eq. (1) as is Eq. (2),

$$k_{eff,V}^{aniso} = \frac{Q_V A_V}{Q_H A_H} k_{eff,H}^{aniso} \sim 3.10\, k_{eff,H}^{aniso} \quad (2)$$

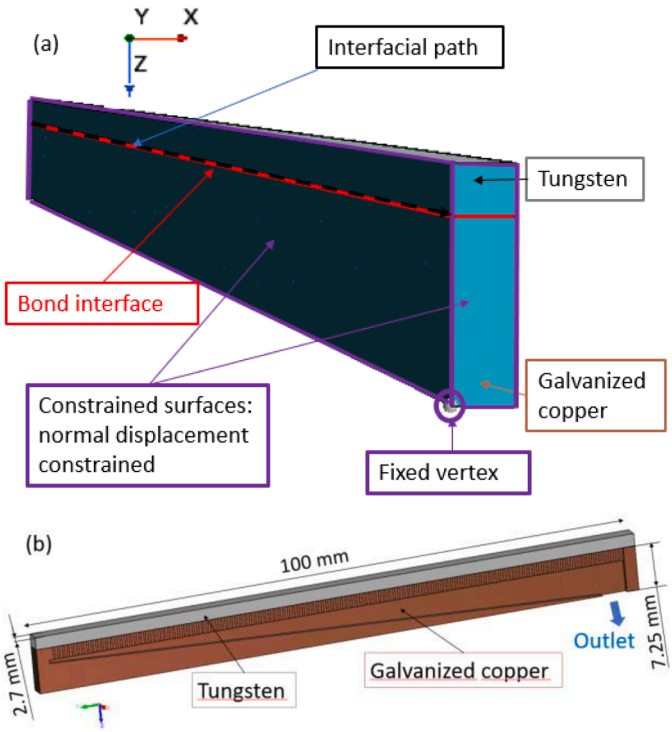


**Fig. 5.** (a) Simple array where the mechanical constraints are highlighted. (b) MCs-array, schematic 3D view.

Performing several simulations with different anisotropic conductivity values, the total error on the heated surface in Eq. (3) has been computed and minimized to find the best fit, as shown in Fig. 4. The H value turns out to be 20.75 W/m/K, and the V one is easily computed by (2).

$$\varepsilon_{tot} = \varepsilon(\Delta T_{ave,0}) \times \varepsilon(\Delta T_{max,0}) \times \varepsilon(\Delta T_{min,0}) \quad (3)$$

### 2.2. Thermo-mechanical approach and model verification

The plasma-facing components (PFCs) of fusion reactors, as the tiles considered in this work, are typically characterized by duplex joint structures [12], that experience significant thermal stresses due to the material properties mismatch and thermal gradient between the heated surface and the cooling channel [13]. The highest stress concentration is at the bond interface, the interface between the plasma-facing material (PFM) and the heat sink (HS) [14]. The interfacial stresses responsible for structural integrity are the delamination (or peeling) and shear stresses [15]; they act respectively normally and tangentially to the surface. The most critical area is the free surface edge where the interfacial stresses reach a peak (stress singularity) with a high risk of interfacial debonding [12]. Finite element modeling (FEM) is used to predict the interfacial stresses behavior; compared to the analytical models, the results are grid-independent except at the free edge where a high mesh dependency occurs; decreasing the mesh size, the interfacial stresses reach higher values [16].

To validate the thermo-mechanical analysis that will be performed on the SM, a 3D finite element stress analysis is performed on a typical PFC, characterized by the same layer structure of an array (half inlet and half outlet manifolds, named “simple array”, with no cooling ducts inside) as shown in Fig. 5a; the results are compared with results reported in [12] and [16]. A uniform temperature load of 350 K is applied on the heated surface; the constraints are applied accounting for similarity to reality avoiding local stresses intensification. The boundary conditions, highlighted in the green boxes in Fig. 5a, are as follows: all the components of the displacement field of a vertex set to zero (fixed vertex);

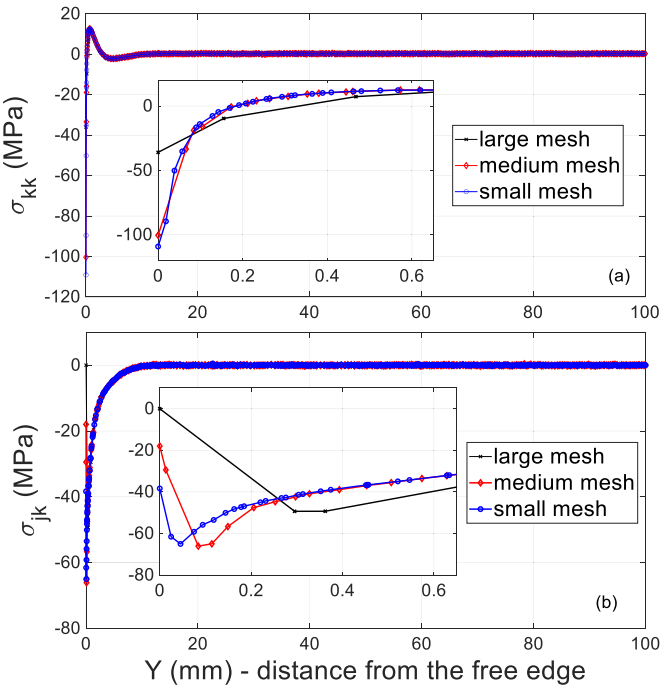


**Fig. 6.** Simple array: delamination or peeling stresses (a) and shear stresses (b) along the interfacial path; zooms of the free surface edge is reported in the insets, highlighting the high mesh dependency.

the displacement in the normal direction of two surfaces constrained, while in the other two directions is free (constrained surfaces). The two materials, tungsten, and galvanized copper are considered as isotropic linear elastic. The mesh is generated using quadratic tet10 elements (tetrahedral elements with the mid-side nodes, not shown). Mesh refinement is implemented at the free edge, where the interfacial path commences, using three distinct mesh size values: large, medium, and small.

The results are analyzed in terms of stress distribution along a path of the bond interface (see Fig. 5a), with the origin ($y = 0$) located at the free surface edge. The normal component to the bond interface $\sigma_{kk}$ and the shear stress component $\sigma_{jk}$ are extracted, corresponding respectively to the interfacial delamination (or peeling) stresses and the interfacial shear stresses. The results of the simple array are shown in Fig. 6. As expected, there is a stress intensification at the free edge where the delamination peak (compressive since the thermal load is positive [12]) reaches higher values decreasing the mesh size. The same is true for the shear stress peak. Note that the shear stresses must be zero analytically since there is no load or constraint applied onto the free surface. The zero-boundary condition at the free edge is almost respected only by the larger mesh size applied. The qualitative behavior of the computed stress is confirmed by the comparison to the results in [16] (not shown).

## 3. Validation

To validate the SM model developed in [8] and calibrated in Section 2.1, a larger spatial scale is now considered; in particular, an entire MCs manifold, consisting of an array of 120 MCs and the surrogate model, consisting of a PS-array of 20 blocks, are analyzed. The inlet and outlet manifolds of these arrays are symmetrically halved. The MCs-array is reported in Fig. 5b, while the PS-array is the same but with the PS blocks replacing the MCs (similarly to Fig. 3). The validation process commences with a thermal assessment, where a mass flow rate of 100 g/s at 300 K and an outlet pressure of 10 bar are applied. A uniform heat flux of 15 MW/m$^2$, previously established through calibration, is imposed, and a comparison to the case with a heat flux of 10 MW/m$^2$ (target heat flux) is carried out. The resulting temperature map is utilized as the thermal load for thermo-mechanical validation.

### 3.1. Thermal validation

Along the arrays, the heat penetration is evaluated as temperature increase in the mockup components, evaluated with respect to the fluid inlet temperature, as a function of the distance from the heated surface. In Fig. 7, three different regions are considered: the hotspot temperature, a region close to it, and far from it. The PS-model exhibits a tendency to overestimate temperatures, particularly within the hotspot region (Fig. 7c). This overestimation can be regarded as a safety factor when applied for engineering purposes, given that the PS-model serves as an equivalent model. In the remaining two regions (Fig. 7d and Fig. 7e), the temperature overestimation gradually decreases until the far region, where the PS-model aligns perfectly with the MCs- model's temperature estimations. This behavior is true for both heat flux scenarios (15 MW/m$^2$ and 10 MW/m$^2$), confirming the quality the calibration. Ultimately, it is shown that the temperature at the interface

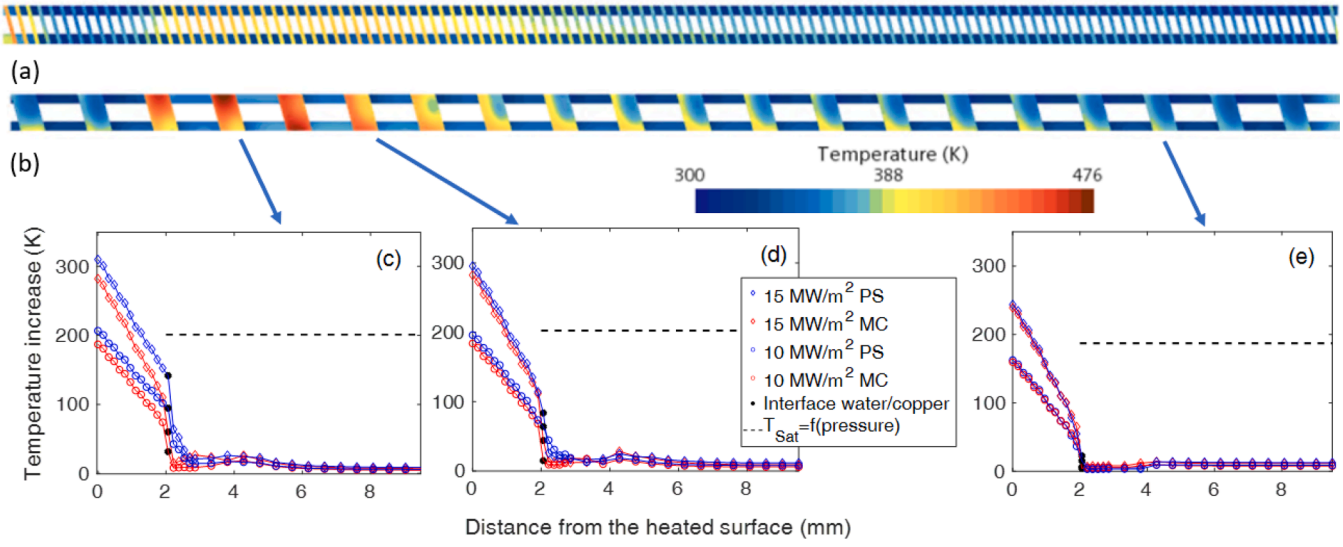


**Fig. 7.** MCs (a) and PS (b) arrays: temperature increase on various mockup regions with respect to the distance from the heated surface, in the hotspot region (c), close to it (d), and far from it (e), respectively.

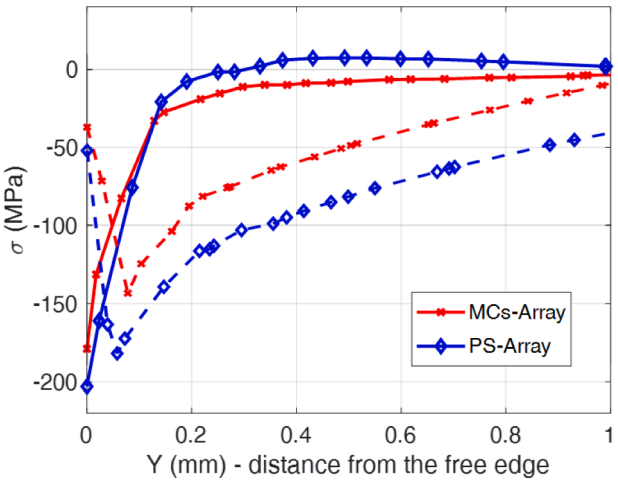


**Fig. 8.** PS and MCs array: delamination or peeling stresses (solid lines) and shear stresses (dashed lines) close to the free surface edge region.

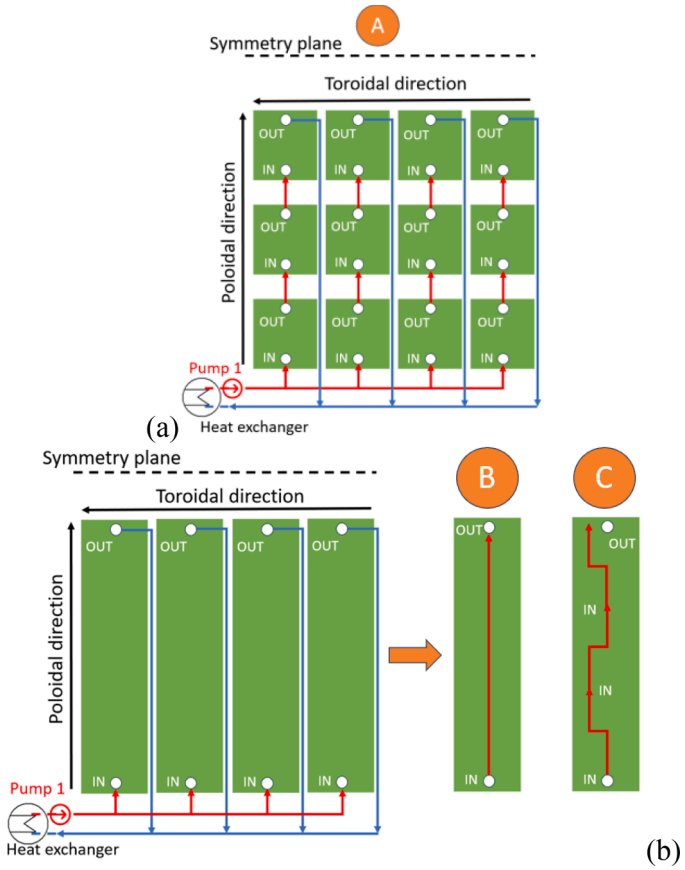


**Fig. 9.** Hydraulic scheme of configuration A (a), 8 parallel paths connecting 3 tiles in series poloidally, and of the alternatives B and C (b).

fluid-copper is below the saturation temperature (187÷202 °C), computed as a function of the absolute pressure, ensuring absence of local boiling, and, a fortiori, of bulk boiling.

### 3.2. Thermo-mechanical validation

The thermos-mechanical analysis applied to the "simple array" above is applied here considering the MCs and PS arrays. The temperature is not uniform anymore in the solid domain, as the temperature maps are extracted from the finite volume mesh used in the conjugate heat transfer analyses ($\dot{m} = 100$ g/s $\dot{Q} = 15$ MW/m$^2$) and imported on the finite element mesh used for the thermo-mechanical analyses. Concerning the mesh, only the medium mesh size of the simple array study is used, as a compromise between the computational cost and stress peaks convergence. The results are reported in Fig. 8 in terms of comparison of the interfacial stresses at the free surface edge, being, as previously described, the most critical domain for structural integrity. Both the delamination (or peeling) and shear stresses are slightly overestimated by the PS-model, in complete agreement with the temperature overestimation, allowing conservative simulation. Both delamination and shear stresses tend to zero already at 1 mm from the free edge.

**Table 2**
Mass flow rate ($\dot{m}$), pressure drop ($\Delta p$), and max heat flux ($\dot{Q}$) to avoid boiling of the configurations A, B, and C.

| Configuration | $\dot{m}\ \left(\frac{kg}{s}\right)$ | $\Delta p\ (bar)$ | $\dot{Q}_{max}\ \left(\frac{MW}{m^2}\right)$ |
|---|---|---|---|
| A | 1.19 | 14.7 | 8.5 |
| B | 1.25 | 6.1 | 8.2 |
| C | 1.25 | 9.4 | 8.8 |

## 4. Design of an entire tile

The PS-model is finally used to evaluate the tiles arrangement in the TM of 600 mm (poloidally) × 400 mm (toroidally). The operational constraints are single-phase flow, total pressure drop of 15 bar, and mass flow rate of 5 kg/s (one single pump) [17]. According to the TM dimensions, a maximum of 4 tiles can be connected in the toroidal direction, and up to 6 tiles can be connected in the poloidal direction. Different configurations have been evaluated, but the most suitable one is composed of 8 parallel paths connecting poloidally 3 tiles in series reaching a total pressure drop of 14.7 bar and a total mass flow rate of 9.5 kg/s (1.19 kg/s per tile) requiring a second pump; this configuration, reported in Fig. 9a, is named as "configuration A" in this work. This configuration is analyzed with the SM, considering that only one tile at a time could be heated by the plasma. Configuration A turns out to be able to stand a maximum heat flux of 8.5 MW/m$^2$ remaining in a single-phase flow, which is below the target of 10 MW/m$^2$.

The two alternative configurations in Fig. 9b have been also assessed with the SM. In Configuration B (single tile with long manifolds), the three series-connected tiles are replaced by a single tile through tapered manifolds. In configuration C (single tile with short manifolds), the inlet manifolds are linked to the outlet one mimicking the manifold connection of three single tiles in series. Note that in this case the PS along the array are in a hybrid parallel-series connection. Both these two configurations result in a notable reduction in pressure drop, reducing the minor losses in the entrance/exit distributing manifolds. Assuming the presence of two water pumps, it becomes possible to slightly increase the mass flow rate to 1.25 kg/s per tile. Configuration B yields a total pressure drop of 6.1 bar, accommodating a heat flux of 8.2 MW/m$^2$ in single-phase flow. On the other hand, configuration C results in total pressure drops of 9.4 bar and 8.8 MW/m$^2$, respectively. The results are reported in Table 2.

Since the divertor's heat load capacity is limited to a 10 cm poloidal width [17], in configurations B and C, the 10-cm segment most vulnerable to overheating must be identified. This entails examining the inlet and outlet manifolds with the lowest cooling capacity, analyzing the channels along these pathways, and pinpointing those segments where the water mass flow rate is at its minimum within that critical 10 cm span. The tungsten temperature profile along the tile at the location corresponding to the longitudinal array with the minimum mass flow rate, when the heat is applied in the most critical 10 cm along the array, is shown in Fig. 10. The hotspots are quite similar for configurations B and C, notwithstanding the small difference in the applied load. Note,

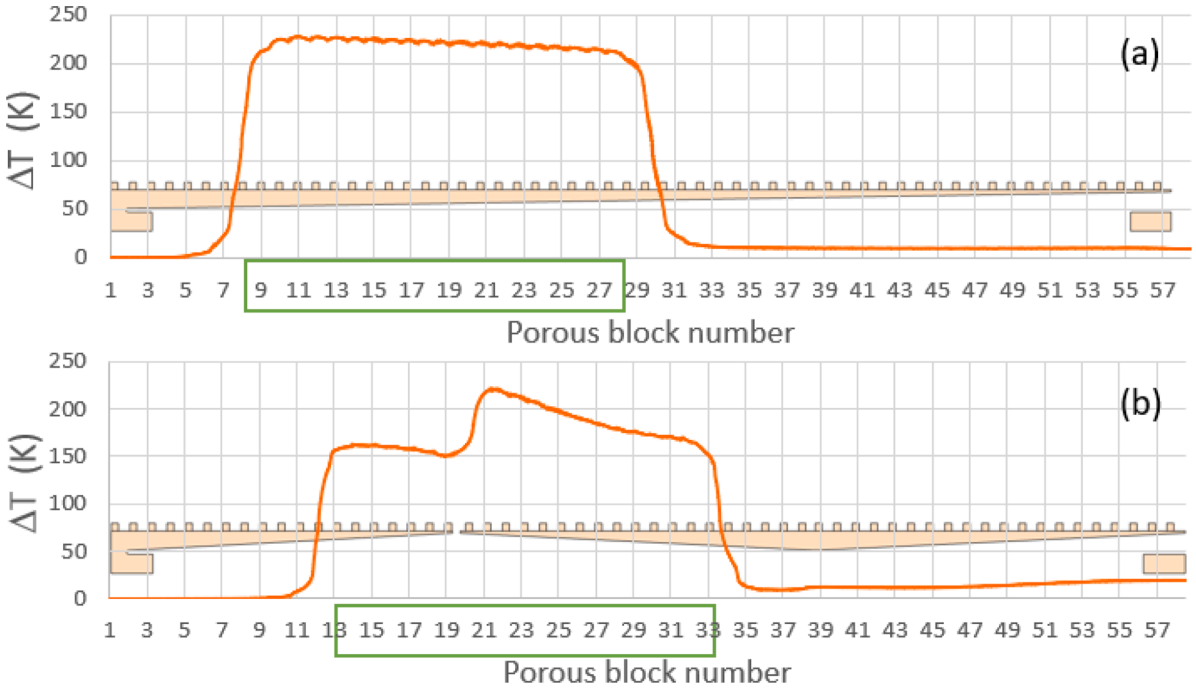


**Fig. 10.** Temperature profile along the tungsten surface, along the least cooled manifolds, for configuration B (a) and C (b), respectively. The heat load is deposited on the most critical 10-cm length (highlighted in the green rectangles). The corresponding manifold layout along the array is also sketched (inlet manifold in (a), and hybrid inlet/outlet manifold in (b)).

however, that the shape of the temperature profile is quite different. While in configuration B the temperature profile matches qualitatively the load shape, in configuration C the tungsten temperature increases in two steps, corresponding to the fact that the fluid can be heated once when it passes through the first bunch of PS, and then a second time when it passes through the second PS bunch. Note also that the hot spots are far from the edges, and delamination and stresses should be negligibly small (see above).

## 5. Conclusions

In this study an equivalent porous strip (PS) model has been calibrated and validated for the thermal-hydraulic and thermo-mechanical behavior of a new divertor tile for W7-X, showing good agreement with the detailed full micro-channel (MC) model. The surrogated model overestimates the temperature, with a maximum of 30 K overestimation in the hotspot region. Ultimately, the PS-model has been used to design alternative configurations for the W7-X divertor target module, exhibiting the capability to bear heat fluxes up to 8–9 MW/m$^2$ keeping the water coolant in a single phase, with a pressure drop from 6 bar to 15 bar.

## CRediT authorship contribution statement

**Francesco Carrone:** Writing – original draft, Visualization, Validation, Software, Formal analysis. **Rosa Difonzo:** Writing – original draft, Validation, Formal analysis, Data curation. **Joris Fellinger:** Writing – review & editing, Supervision, Methodology, Funding acquisition. **Laura Savoldi:** Writing – review & editing, Supervision, Resources, Project administration, Methodology, Funding acquisition, Conceptualization.

## Declaration of competing interest

The authors declare that they have no known competing financial interests or personal relationships that could have appeared to influence the work reported in this paper.

## Data availability

No data was used for the research described in the article.

## Acknowledgments

The authors are grateful to Mr. H. Ebadi for the support in producing Fig. 1 and to Prof. A. Cammi for helping in the document revision. This work has been partially carried out within the framework of the EUROfusion Consortium, partially funded by the European Union via the Euratom Research and Training Programme (Grant Agreement No 101052200 — EUROfusion). Views and opinions expressed are however those of the author(s) only and do not necessarily reflect those of the European Union, the European Commission. Neither the European Union nor the European Commission can be held responsible for them. Computational resources provided by hpc@polito, which is a project of Academic Computing within the Department of Control and Computer Engineering at the Politecnico di Torino (http://www.hpc.polito.it)

## References

[1] "Fusion for a cleaner, reliable and self-sufficient energy mix - Fusion for Energy." Accessed: Mar. 07, 2023. [Online]. Available: https://fusionforenergy.europa.eu/news/fusion-for-a-cleaner-reliable-and-self-sufficient-energy-mix/.
[2] D. Lerede, M. Nicoli, L. Savoldi, A. Trotta, Analysis of the possible contribution of different nuclear fusion technologies to the global energy transition, Energy Strategy Reviews 49 (2023) 101144, https://doi.org/10.1016/j.esr.2023.101144. Sep.
[3] "Wendelstein 7-X | Max-Planck-Institut für Plasmaphysik." Accessed: Mar. 07, 2023. [Online]. Available: https://www.ipp.mpg.de/w7x.
[4] J. Boscary, et al., Conceptual design of the next generation of W7-X divertor W-target elements, Fusion Eng. Des. 192 (2023) 113629, https://doi.org/10.1016/j.fusengdes.2023.113629. Jul.
[5] J. Boscary, et al., Design and technological solutions for the plasma facing components of WENDELSTEIN 7-X, Fusion Eng. Des. 86 (6–8) (Oct. 2011) 572–575, https://doi.org/10.1016/J.FUSENGDES.2010.11.020.

[6] J. Boscary, et al., Completion of the production of the W7-X divertor target modules, Fusion Eng. Des. 166 (2021) 112293, https://doi.org/10.1016/j.fusengdes.2021.112293. May.
[7] J. Boscary, et al., Actively Water-Cooled Plasma Facing Components of the Wendelstein 7-X Stellarator, Fusion Sci. Technol. 64 (2) (2013) 263–268, https://doi.org/10.13182/FST12-499. Aug.
[8] H. Ebadi, et al., A multi-scale hybrid approach to the modelling and design of a novel micro-channel cooling structure for the W7X divertor, Case Studies in Thermal Engineering 42 (2023) 102734, https://doi.org/10.1016/j.csite.2023.102734. Feb.
[9] M. Cagnoli, A. Froio, L. Savoldi, R. Zanino, Multi-scale modular analysis of open volumetric receivers for central tower CSP systems, Sol. Energy 190 (2019) 195–211, https://doi.org/10.1016/j.solener.2019.07.076. Sep.
[10] H. Greuner, B. Boeswirth, J. Boscary, P. McNeely, High heat flux facility GLADIS, J. Nucl. Mater. 367–370 (2007) 1444–1448, https://doi.org/10.1016/j.jnucmat.2007.04.004. Aug.
[11] "Getting Started." Accessed: Mar. 24, 2023. [Online]. Available: https://docs.sw.siemens.com/documentation/external/PL20211129219030255/en-US/userManual/starccmp_userguide_html/index.html#page/STARCCMP%2FGUID-44BC55FD-ACDE-47F1-A792-C904A5A45CAD.html%23.
[12] J.H. You, H. Bolt, Analysis of singular interface stresses in dissimilar material joints for plasma facing components, J. Nucl. Mater. 299 (1) (2001) 1–8, https://doi.org/10.1016/S0022-3115(01)00680-8. Oct.
[13] J.H. You, H. Bolt, Thermal stress intensity factor of interfacial cracks of a plasma facing component under high heat flux loading, Fusion Eng. Des. 65 (4) (2003) 483–492, https://doi.org/10.1016/S0920-3796(03)00051-6. Jul.
[14] S. Timoshenko, Analysis of Bi-Metal Thermostats, J Opt. Soc. Am. 11 (3) (1925) 233, https://doi.org/10.1364/JOSA.11.000233. Sep.
[15] E. Suhir, Interfacial Stresses in Bimetal Thermostats, J. Appl. Mech. 56 (3) (1989) 595–600, https://doi.org/10.1115/1.3176133. Sep.
[16] X.-F. Wu, R.A. Jenson, Stress-function variational method for stress analysis of bonded joints under mechanical and thermal loads, Int. J. Eng. Sci. 49 (3) (2011) 279–294, https://doi.org/10.1016/j.ijengsci.2010.11.005. Mar.
[17] J. Fellinger, et al., Tungsten based divertor development for Wendelstein 7-X, Nuclear Materials and Energy (2023) 101506, https://doi.org/10.1016/j.nme.2023.101506. Sep.